SiGe Circuits for Spread Spectrum Automotive Radar

Saverio Trotta[1, 3], Bernhard Dehlink[2,3], Herbert Knapp[2], Klaus Aufinger[2], Thomas F. Meister[2], Josef Böck[2], Werner Simbürger[2], and Arpad L. Scholtz[3]

[1] Now with Freescale Semiconductor GmbH, Schatzbogen 7, D-81829 Munich, Germany
[2] Infineon Technologies AG, Am Campeon 1-12, D-81726 Munich, Germany
[3] Vienna University of Technology, Karlsplatz 13, A-1040 Vienna, Austria
E-mail: Saverio.Trotta@freescale.com

Abstract — **This paper presents circuits in SiGe bipolar technology for spread spectrum automotive radar applications in the band from 77 to 81 GHz. They cover the transmit and receive paths. The transmitter integrates a voltage controlled oscillator, a prescaler by 64, a 10 bit linear feedback shift register (LFSR), and a biphase modulator. The system has been optimized in order to achieve a range resolution less than 12 cm and an unambiguous range of 124 m. The quadrature receiver frontend consists of a single–ended low-noise amplifier (LNA), balanced-to-unbalanced converters, two fully differential direct-conversion mixers, LO buffer amplifiers, and a branchline coupler for I/Q generation. The presented systems show that millimeter-wave circuits in SiGe technology can achieve high integration levels along with high performance. They are well suited for application in spread spectrum automotive radar systems.**

Figure 1. Simplified architecture of a spread spectrum transmitter.

I. INTRODUCTION

In a spread spectrum system the transmitted signal is spread over a frequency band, which is much wider than the minimum bandwidth required to transmit the information [1]. Automotive radar systems can take advantage of spread spectrum techniques because of their interference rejection, immunity from noise and multipath distortion, and high resolution ranging properties. In addition, there is no need for high-speed, fast-settling frequency synthesizers. Moreover, spread spectrum techniques can improve the reliability of automotive radars. The data from different sensors on different cars can be combined in order to observe the complete car environment. Thus a spread spectrum radar system will allow to share the same bandwidth also for data-link needed by car-to-car communication systems [2].

Pseudo noise (PN) signal processing along with direct-sequence modulation has been widely used for developing powerful spread spectrum ranging systems. These concepts are also well suited for short-range automotive radar applications in the 79 GHz band. A simplified transmitter architecture is shown in Fig. 1. The spread spectrum signal is generated by means of direct sequence technique: the carrier is modulated with a pseudo noise sequence (code). Compared to other spread spectrum systems, pulse radar for example, the PN-radar allows to lower the maximum output power level of the transmit signal because it is continuously active. For short-range applications (e.g. 1 to 30 meter), there is the need to use ultra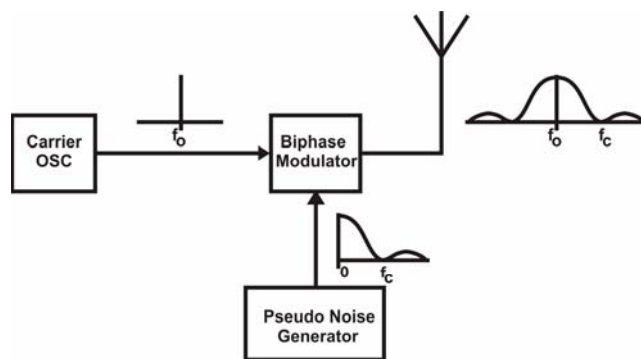-wideband (UWB) techniques since there is a direct relation between the bandwidth of the transmit signal (f_C in Fig. 1) and the achievable range resolution d_{min} [3,4]:

$$d_{min} \leq c/2f_C, \tag{1}$$

where c is the speed of light. Another performance characteristic of a ranging system is the supported unambiguous range d_{max}, which is the maximum distance that the system is able to detect:

$$d_{max} \leq c/2T_P, \tag{2}$$

where $T_P = N/f_C$ is the period of the pseudo random sequence and N the number of bits. In order to keep the range resolution small and at the same time support large unambiguous range, the chip duration $T_C = 1/f_C$ is required to be small while N has to be sufficiently large. For the system presented in this paper, $N = 1023$ and $f_C = 1.235$ GHz have been chosen in order to achieve a d_{max} of approximately 124 m and a d_{min} of less than 12 cm. Moreover, in ranging systems based on spread spectrum techniques, a large value for N is also needed to improve the peak of the autocorrelation function and lower the cross-correlation function. This allows the receiver to discriminate among spread spectrum signals generated by different sequences [10]. Considering a 79 GHz carrier signal and a speed of 100 km/h, the Doppler signal is approximately 14.5 kHz. This is much lower than the PN-code repetition frequency of 1.2 MHz (which represents the spacing between the discrete lines in the spectrum of the PN-signal) and therefore does not deteriorate the correlation response of the receiver in the PN-radar [5].
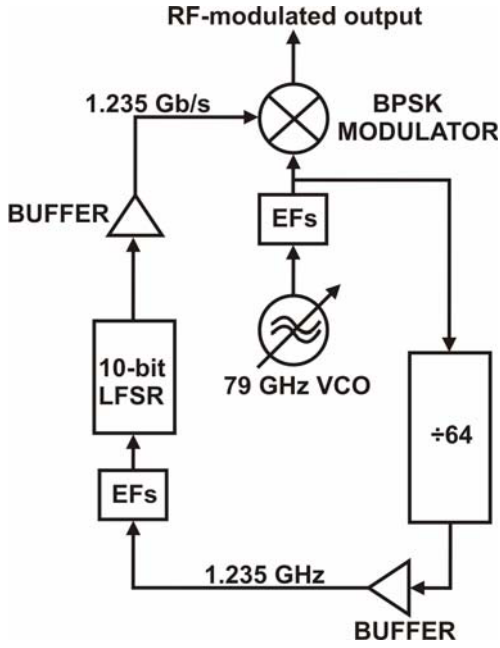
Figure 2. Block diagram of the transmitter.

Various radar systems require the use of in-phase and quadrature signals for the determination of the distance of the target and its relative velocity. In pulsed Doppler-radar systems, the received signal and the reference signal can be out-of-phase such that coherent detection results in zero output. No information about the target's relative velocity can therefore be extracted [6]. A second branch that is shifted in phase by 90° yields the desired information in that case. The combination of both in-phase (0°, I) and quadrature (90°, Q) components using $\sqrt{S_I^2 + S_Q^2}$ results in no loss of information. Spread-spectrum radar systems correlate the received signal with the reference PN-sequence to measure the distance to the target. The delayed reference and the incoming signal are incoherent, therefore the correlation can also yield zero output. For that case, the correlation with I and Q versions of the received signal is needed [7].

II. CIRCUIT DESIGN

A. Transmitter

The block diagram of the spread-spectrum transmitter chip is shown in Fig. 2. The system is fully differential and consists of four main blocks: a 79 GHz VCO, a prescaler, a biphase modulator, and a pseudo-noise sequence generator. The clock signal which drives the PN-source is generated on the same chip. The VCO is based on the chip presented in [8] and has a center frequency of 79 GHz. The differential signal generated by the VCO drives the biphase modulator and the prescaler.

The prescaler is used to downconvert the VCO signal to 1.235 GHz. It consists of six divider stages. The first stage is a dynamic frequency divider. Dynamic frequency dividers achieve higher operating frequencies than static frequency dividers at comparable or lower power dissipation. Therefore they are an attractive choice for the first stage of a frequency divider chain at the output of the 77-GHz VCO. In contrast to injection-locked dividers, which suffer from a narrow locking
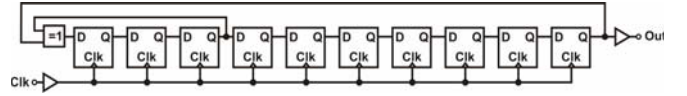

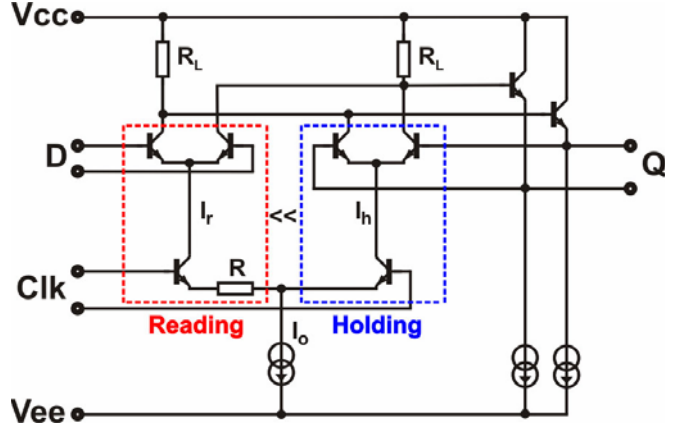Figure 3. A 10 stages pseudo random bit sequence generator.
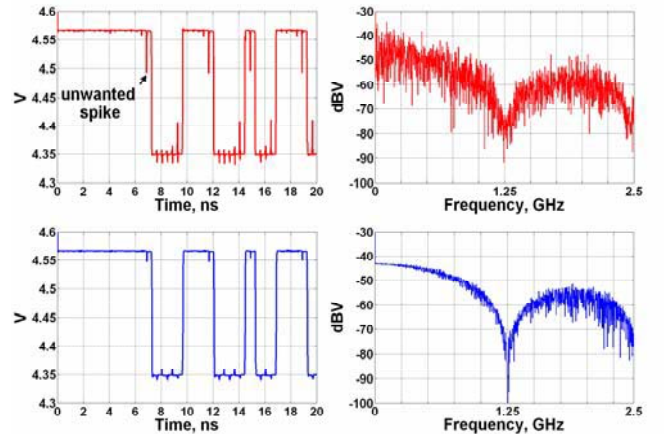

Figure 4. Latch schematic.

Figure 5. Simulation results of the PRBS: effect on the spectrum due to spikes in the pseudo noise signal. The quality of the output signal can be improved (lower figures) by using the resistor R in the latch.

range, regenerative dividers are able to operate over a frequency range of approximately 3:1. This provides sufficient margin to prevent a reduction of the usable VCO tuning range [9]. The other five stages are static dividers optimized for low power consumption. Since the signal from the prescaler has to drive all the clocked stages in the PN-generator, a buffer has been connected at the output of the last divider stage.

The PN-sequence is generated by a full-rate pseudo random bit sequence (PRBS) generator (Fig. 3). The chip rate of the PN-sequence is 1.235 Gb/s. Since ≈ 90 % of the signal power of the PN-sequence is contained in the main lobe, the spread spectrum system will require a bandwidth of approximately 2.5 GHz. The PRBS generator consists of a clock input stage, a linear feedback shift register (LFSR) [1,10], and an output buffer. Three cascaded emitter followers are used in the clock input stage in order to shift down the DC level of the clock signal and drive the LFSR. The shift register contains $n = 10$ stages and generates a maximum-length

sequence of $N = 2^n - 1 = 1023$ bits. The maximum-length sequence (M-sequences) are the longest codes generated by a given shift register. They have good autocorrelation property [1, 10]. With a 10 stage LFSR it is possible to generate 10 different M-sequences [1]. The sequence of the PRBS is set by the output signals from the 10 stages which are fed back and applied to the first stage via an XOR. By using a multiplexer it is possible to select the feedback lines and thereby set the sequence. In this way, radars mounted on different cars can transmit different sequences avoiding potential interferences. In our first test chip, we did not implement the multiplexer. In this case the sequence is generated by the feedback signals from the third and the last stages (Fig. 3). Each stage in the PRBS is a delay element which has been implemented as a flipflop. The performance of the overall system at 79 GHz strongly depends on the quality of the baseband PN-signal and it is quite challenging to integrate baseband together with high-frequency blocks. Recently, new techniques have been presented to improve the performance of flip-flops connected in a divider configuration [11,12]. Such techniques are based on asymmetric current levels in the reading and holding paths in each latch. This asymmetry leads to a longer reading time against a shorter holding time which makes the flip-flop faster. In order to improve the shape of the output signal from the PRBS, in our design the concept of asymmetry has been used, but in the opposite way. As shown in Fig. 4, in each latch a resistor has been placed in the reading path to unbalance the tail current I_o in the holding path. In this way, the holding time will be longer than the reading time. Because of this asymmetry, spikes in the output signals are avoided during clock transitions, as shown in Fig. 5. In the third stage another differential pair has been also implemented to force the initial condition in the LFSR. In order to achieve a fast switching behavior at the upper differential pairs of the modulator, an output buffer has been integrated in the PRBS to achieve a maximum differential output swing of 1.4 V_{pp}.

The biphase modulator shifts the baseband spectrum of the PRBS to the carrier frequency. The fully differential biphase modulator is implemented as a Gilbert cell and shown in Fig. 6. The lower differential pair of the modulator is driven by the 79 GHz carrier and the upper pairs by the PN-signal. Since the bit rate of the PN-signal is very low compared to the frequency of the carrier, the modulator works mostly as a cascode thereby improving the performance. Transmission lines are used as load in the modulator and also for on-chip matching.

B. Quadrature receiver

The quadrature receiver frontend consists of a single-ended low-noise amplifier (LNA), balanced-to-unbalanced converters to transform the single-ended signal to differential signals, two fully differential direct-conversion mixers, LO buffer amplifiers, and a branchline coupler [13]. An overview of the implemented circuit is depicted in Fig. 7.

The design of the LNA is similar to the one presented in [14]. It consists of three common-emitter (CE) stages, the first one is shown in Fig. 8. Stages two and three basically have the same topology. The input of the LNA is matched with transmission lines for a return loss larger than 10 dB
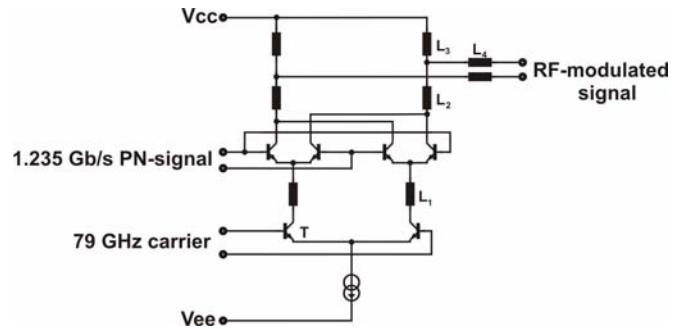

Figure 6. BPSK-modulator schematic. L_1, L_2, L_3 and L_4 are microstrip-line elements, all with inductive behavior.
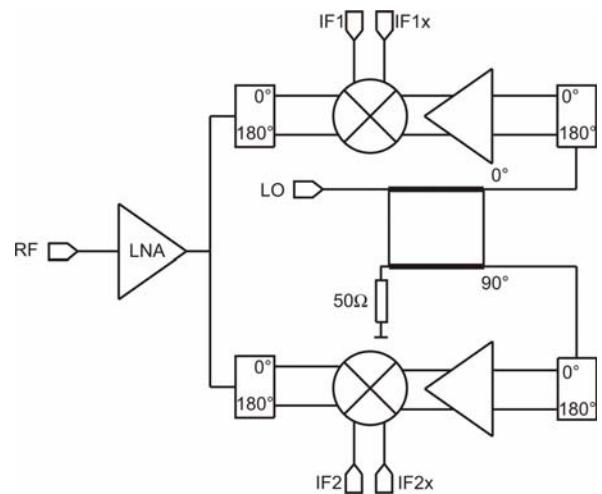

Figure 7. Block diagram of the IQ frontend.

(VSWR < 2 : 1). The simulated noise figure of the LNA is 6.5 dB in the frequency range from 75 GHz to 86 GHz. Interstage matching is accomplished by an LC matching network (L_2, C_3). Here, the inductance is replaced by a transmission line that is shorted for high frequencies. The transformed input impedance of the following stage determines the load impedance (the gain) of the CE transistor Q_1. The output of the LNA is matched with transmission lines to a 50 Ω interface, taking into account the parasitic pad capacitance. The measured gain of a stand-alone version of the LNA is 12 dB. The LNA consumes 32 mA.

The power splitting of the RF signal is done as follows: Two transmission lines of 220 μm length transform the input impedance of both RF baluns to a low impedance. This value is transformed to the 50 Ω interface by a series transmission line and a shunt capacitor.

The RF and LO baluns are LC–baluns (Fig. 9) where the inductors are replaced by transmission lines [15]. With this type of balun, a single-ended to differential conversion and impedance matching is achieved simultaneously. The insertion loss of one balun is 1.6 dB.

The direct-conversion mixers are based on the high-level mixer presented in [16]. The mixer is designed for high impedance external loads, so the internal load of 2 × 400 Ω
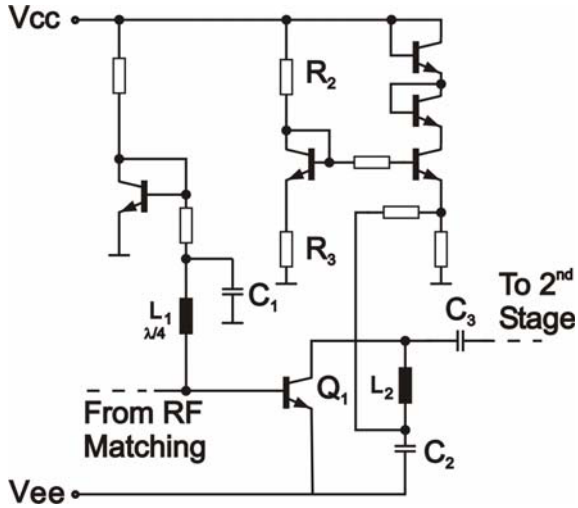
Figure 8. One stage of the low-noise amplifier. L_1 and L_2 are microstrip-line elements, all with inductive behavior.
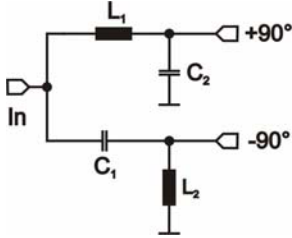

Figure 9. Schematic diagram of the balun. L_1 and L_2 are microstrip-line elements, all with inductive behavior.

and the bias current of 6 mA determine the conversion gain. The simulated noise figure of one mixer is 12 dB, and the conversion gain is 24 dB. The current consumption of one mixer, including biasing, is 11 mA.

To maintain a high voltage swing at the LO port of the mixer, which is essential for good noise performance, the LO signal is applied to the four switching transistors via an LO buffer. The simulated gain of the buffer is 10 dB in the frequency range around 80 GHz. The buffers consume 60 mA each.

The 0° / 90° phase shift between the two IF output ports is achieved by the use of a branchline coupler at the LO port of the front-end. The isolated port of the coupler is terminated with 50 Ω to broaden the coupler's bandwidth. Transmission lines match the input impedance of the coupler to 50 Ω, taking into account the parasitic pad capacitance. The four branches have a length of 480 μm each, which equals λ / 4 at 80 GHz.

III. TECHNOLOGY

The chips are manufactured in an advanced 200 GHz f_T SiGe:C bipolar process based on the technology presented in [17]. The transistors achieve the highest f_T at a current density of 5 mA/μm². Shallow and deep trench isolation are used. The transistors are fabricated with a double–polysilicon self-aligned emitter-base configuration with a SiGe:C base. This base is integrated by selective epitaxial growth. The transistors
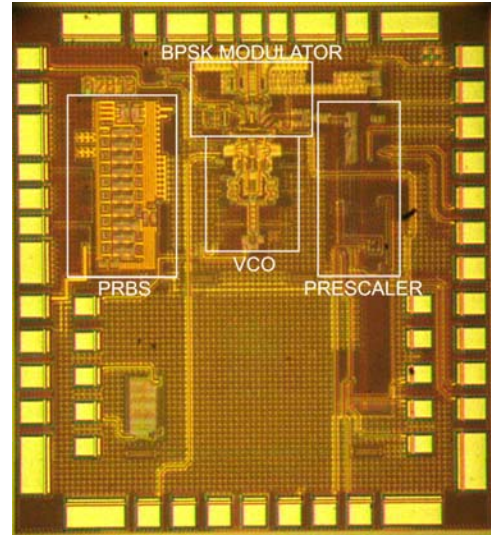

Figure 10. Chip photo of the spread spectrum transmitter (1128×1028 μm²).

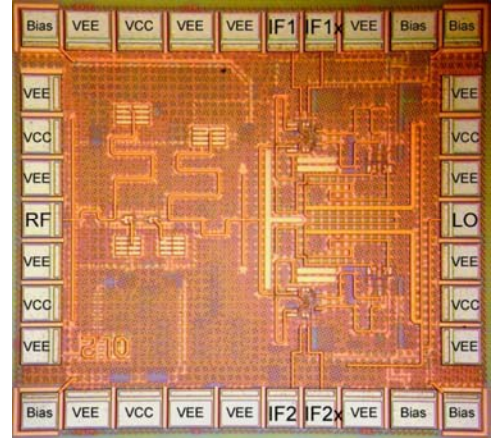Figure 11. Chip photo of the quadrature receiver (1100×1000 μm²).

have a minimum emitter mask width of 0.35 μm, resulting in an effective emitter width of 0.18 μm. The technology additionally features high-voltage transistors with a BV_{CEO} of 5.0 V [18]. Four metal layers, MIM-capacitors, varactors, and different types of resistors are also included. The chip photograph is depicted in Fig. 10 and 11. The size of the chip is 1128×1028 μm² for the spread spectrum transmitter and 1100×1000 μm² for the quadrature receiver.

IV. MEASUREMENT RESULTS

All measurements were performed on-wafer with probes. The temperature was kept at a constant level of 25 °C. All off-chip losses from the measurement setup were de-embedded from the measurement results.

A. Transmitter

The complete spread spectrum transmitter draws 750 mA from a +5.5 V supply. The baseband output from the PRBS was connected to a spectrum analyzer. The RF-modulated signal was connected via a W-band waveguide to a W-band down-conversion mixer, which down-converts the 79 GHz

modulated signal to an IF of 4.646 GHz. This output was applied to a second spectrum analyzer. The measurement results are shown in Figs. 12 and 13. The well-defined shape of the baseband signal validates the technique used in the design of the LFSR. Its quality also determines the precise shape of the up-converted signal, which shows only a small feedtrough of the carrier. The slight asymmetry in the measured spectrum shape of the up-converted signal is due to the variation of the conversion loss of the down-conversion mixer at different IF frequencies. The spectral nulls at $\Delta f = \pm 1.235$ GHz can be clearly seen in the baseband and up-converted signal spectra. The code repetition frequency of the pseudo noise signal is shown in Fig. 14. The measured differential output power of the modulator is +1.5 dBm, which is large enough for short-range applications without an additional power amplifier (PA) stage.

B. Quadrature receiver

The receiver draws 195 mA from a +5.5 V supply. The LO power level was set to deliver +1 dBm to the chip. The mixers are designed for high impedance external loads, thus external voltage followers with an input impedance of 100 kΩ were attached to the output of the mixers. This provides matching to the 50 Ω measurement environment. The differential IF signal was combined with a 180° low-frequency hybrid. The noise figure was measured using HP's 8970B noise figure meter. The single-sideband (SSB) noise figure and the conversion gain are depicted in Fig. 15. At 79 GHz, the noise figure is 11 dB and the conversion gain 32 dB. The 90° phase difference between the in-phase and the quadrature output is a crucial parameter for the performance of precision sensor systems. Measurement results show that the relative phase deviation from 90° is within ±8° from 75 GHz to 88 GHz. Figure 16 shows the conversion gain and noise figure imbalance of the two mixer outputs. The gain differs by less than 0.7 dB. The difference in noise figure is smaller than 0.4 dB. The plot of the differential IF output voltage versus RF input power is shown in Fig. 17. Due to the external high impedance load of the mixer, the output voltage is depicted instead of the output power. The input-referred 1 dB compression point is -19 dBm.

V. Conclusion

In this paper design considerations for SiGe circuits for spread spectrum automotive radar applications in the band from 77 to 81 GHz have been reported. A complete transmitter at 79 GHz with integrated baseband signal generation has been demonstrated. The chip provides +1.5 dBm differential output power, which is enough for short-range radar applications without an additional PA stage. The range resolution is less than 12 cm. The main lobe of the spread spectrum RF signal occupies a bandwidth of ≈ 2.5 GHz. The quadrature receiver features a conversion gain of more than 28 dB and a noise figure of 11 dB over a frequency range from 75 GHz to 86 GHz. The two IF outputs are within 8° of 90° from 75 GHz to 88 GHz. The gain imbalance between these outputs is smaller than 0.7 dB, and the imbalance in noise figure is smaller than 0.4 dB. The input-referred 1 dB compression point is -19 dBm. The performance of these circuits indicates their suitability for precision sensing applications at 79 GHz.
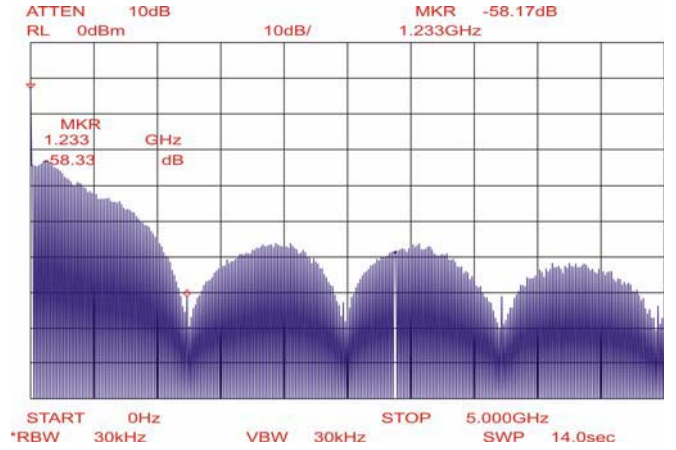

Figure 12. Measured pseudo noise baseband signal spectrum. Spectral nulls at $\Delta f = \pm f_c = 1.235$ GHz.
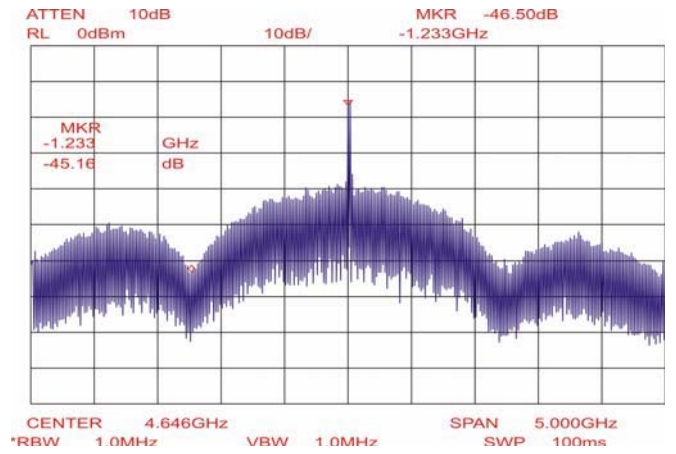

Figure 13. Measured RF-modulated signal spectrum. Free-running VCO; the 79 GHz PN-signal was down-converted to an IF of 4.646 GHz. Spectral nulls at $\Delta f = \pm f_c = 1.235$ GHz.
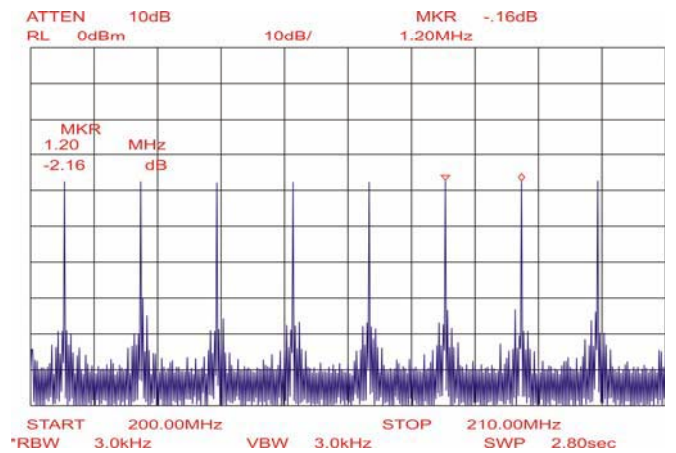

Figure 14. Measured discrete lines of the baseband signal spectrum. The PN-code repetition frequency is $f_c/N = 1.2$ MHz.

From the technology point of view, the obtained results show that very high integration levels in millimeter-wave frequency ranges are feasible in SiGe bipolar technology.

REFERENCES

[1] R.C. Dixon, *Spread Spectrum Systems with Commercial Application*, John Wiley & Sons, 3rd Edition, 1994.

[2] V. Wider, J. Detlefsen, U. Siart, J. Büchlert, and M. Wagner, "Automotive Radar Sensor with Communication Capability," *IEEE ECWT Digest*, pp. 305–308, Oct. 2004.

[3] H. Veenstra, E. van der Heijden, and D. van Goor, "15-27 GHz Pseudo-Noise UWB transmitter for short-range automotive radar in a production SiGe technology," *IEEE Proceedings of ESSCIRC*, pp. 275–278, Sept. 2005.

[4] S. Trotta, H. Knapp, D. Dibra, K. Aufinger, T. F. Meister, J. Böck, W. Simbürger, and A. L. Scholtz, "A 79GHz SiGe-Bipolar Spread Spectrum TX for Automotive Radar," *IEEE ISSCC Digest*, pp. 430–431, Feb. 2007.

[5] J. Detlefsen, E. Schmidhammer, and T. Troll, "Spread Spectrum Ranging for an ACC-Radar," *IEEE Proceeding of ISSSTA*, vol. 3, pp. 994–998, Sep. 1998.

[6] Royal School of Artillery, *Principles of Pulsed Doppler Radar*. Basic Science & Technology Section (BST), pp. H03–1 – H03–16, May 2004.

[7] V. Filimon, and J. Buechler, "A Pre-Crash Radar Sensor System Based on Pseudo-Noise Coding," *IEEE MTT-s Digest*, pp. 1415–1418, June 2000.

[8] H. Li and H.-M. Rein, "Millimeter-Wave VCOs With Wide Tuning Range and Low Phase Noise, Fully Integrated in a SiGe Bipolar Technology," *IEEE J. Solid-State Circuits*, vol. 38, pp. 184–191, Feb. 2003.

[9] H. Knapp, B. Dehlink, H.-P. Forstner, E. Kolmhofer, K. Aufinger, J. Böck, and T. F. Meister, "SiGe Circuits for Automotive Radar," *IEEE SiRF Digest*, pp. 231–236, Jan. 2007.

[10] H.-J. Zepernick and A. Finger, *Pseudo Random Signal Processing –Theory and Application*, John Wiley & Sons, 2005.

[11] Y. Suzuki, Z. Yamazaki, Y. Amamiya, S. Wada, H. Uchida, C. Kurioka, S. Tanaka, and H. Hida, "120-Gb/s Multiplexing and 110-Gb/s Demultiplexing ICs," *IEEE J. Solid-State Circuits*, vol. 39, pp. 2397–2402, Dec. 2004.

[12] S. Trotta, H. Knapp, T. F. Meister, K. Aufinger, J. Böck, W. Simbürger, and A. L. Scholtz, "110-GHz Static Frequency Divider in SiGe Bipolar Technology," *IEEE CSICS Digest*, pp. 291–294, Nov. 2005.

[13] B. Dehlink, H.-D. Wohlmuth, K. Aufinger, F. Weiss, and A. L. Scholtz, "An 80 GHz SiGe Quadrature Receiver Frontend," *IEEE CSICS Digest*, pp. 197–200, Nov. 2006.

[14] B. Dehlink, H.-D. Wohlmuth, K. Aufinger, T. F. Meister, J. Böck, and A. L. Scholtz, "A low-noise amplifier at 77 GHz in SiGe:C bipolar technology," *IEEE CSICS Digest*, pp. 287–290, Nov. 2005.

[15] W. Bakalski, W. Simbürger, H. Knapp, H.-D. Wohlmuth, and A. L. Scholtz, "Lumped and distributed lattice-type LC-baluns," *IEEE MTT-s Digest*, pp. 209–212, June 2002.

[16] H.-D. Wohlmuth and W. Simbürger, "A high IP3 RF Receiver Chip Set for Mobile Radio Base Stations up to 2 GHz," *IEEE J. Solid-State Circuits*, vol. 36, no. 7, pp. 1132–1137, July 2001.

[17] J. Böck, H. Schäfer, K. Aufinger, R. Stengl, S. Boguth, R. Schreiter, M. Rest, H Knapp, M. Wurzer, W. Perndl, T. Böttner, and T. F. Meister, "SiGe bipolar technology for automotive radar applications", *IEEE BCTM Digest*, pp. 84–87, Sept. 2004.

[18] R. K. Vytla, T. F. Meister, K. Aufinger, D. Lukashevich, S. Boguth, H. Knapp, J. Böck, H. Schäfer, and R. Lachner, "Simultaneous Integration of SiGe High Speed Transistors and High Voltage Transistors", *IEEE BCTM Digest*, pp. 61–64, Oct. 2006.
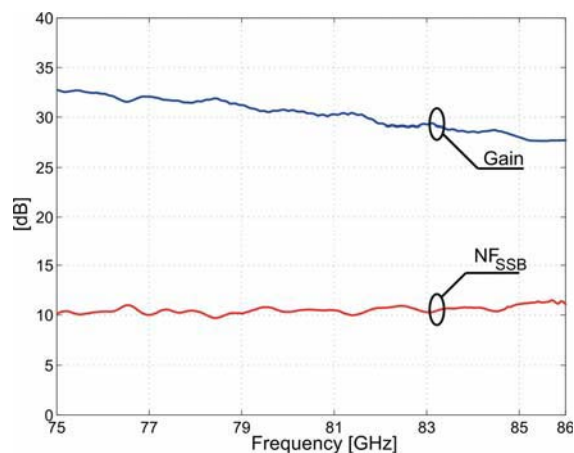
Figure 15. Measured single-sideband noise figure and conversion gain of the quadrature receiver (IF = 10 MHz).
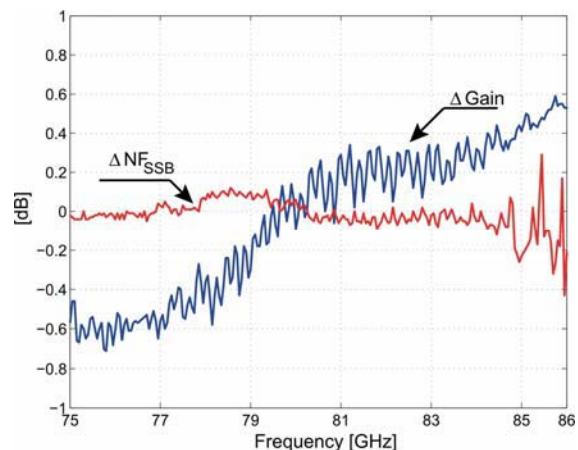

Figure 16. Measured gain and noise figure imbalance of the two output ports (IF = 10 MHz).
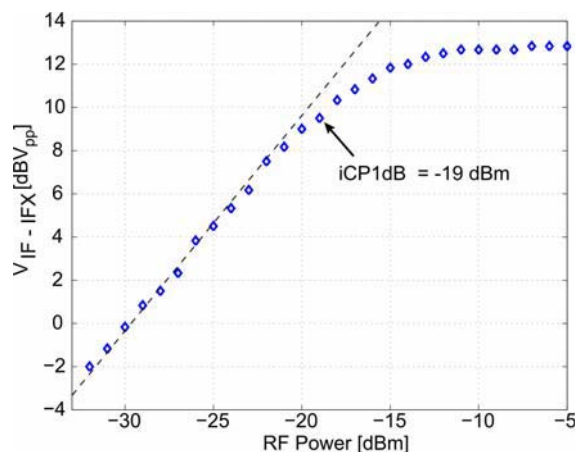

Figure 17. Measured input-referred 1-dB compression point of the quadrature receiver (IF = 10 MHz).